*Manuscript
Click here to view linked References

Climate variability on the south-eastern Tibetan Plateau since the Late Glacial based on a multiproxy approach from Lake Naleng – comparing pollen and non-pollen signals

Authors:

Opitz, Stephan[a*], Zhang, Chengjun[b], Herzschuh, Ulrike[c], Mischke, Steffen[d]

[a] Institute for Geography, University of Cologne, Albertus-Magnus-Platz, 50923 Köln, Germany

[b] School of Earth Sciences & Key Laboratory of Mineral Resources in Western China (Gansu Province), Lanzhou University, Lanzhou, 730000, China

[c] Alfred Wegener Institute for Polar and Marine Research, Telegrafenberg A43, 14473 Potsdam, Germany

[d] Faculty of Earth Sciences, University of Iceland, 101 Reykjavík, Iceland

Corresponding author*:

Stephan Opitz, Institute for Geography, University of Cologne, Albertus-Magnus-Platz, 50923 Köln, Germany, E-Mail: Stephan.Opitz@uni-koeln.de

Highlights:

- Comparison of multi-proxy downcore variations with reconstructed MAP and MAT
- TOC, C/N, $\delta^{13}C_{org}$, CIA and Sr/Ba are related to changes of precipitation
- Doubling of Holocene precipitation in comparison to Late Glacial conditions
- Diminishing moisture availability from south to north on the eastern TP in the Holocene

Keywords: Element concentrations; Grain-size; Principal component analysis; Temperature and precipitation reconstructions; Weathering; Asian monsoon; Tibetan Plateau

Abstract

A multi-proxy Late Glacial environmental record is described from Lake Naleng (31.10°N; 99.75°E, 4200 m above sea level), situated on south-eastern Tibetan Plateau to gain deeper insights into the hydrological and palaeoclimate development since 17.7 cal ka BP. Palynological reconstructions of variations in mean annual precipitation (MAP) and temperature (MAT), sedimentological data and sediment chemistry including weathering indicators provide a multi-faceted picture of local and regional environmental changes since the Late Glacial. Principal component analyses of all parameters provide information on interrelationships between each parameters, which help to evaluate their traceability to temperature and precipitation and to estimate their usability as proxy indicators for local and or regional variations.

During the Late Glacial from 17.7 to 14.0 cal ka BP Lake Naleng experienced cold and dry climate conditions with low biological productivity and supply of unaltered fine-grained material due to the high supply of glacier milk. During the second half of the Late Glacial, climate conditions changed abruptly: increases in MAT (from −4 to −2.2°C) and MAP (from 500 mm to 820 mm) between 14.0 and 13.0 cal ka BP indicate a climate amelioration. This time interval can be correlated to the Bølling/Allerød (B/A) warming period in the North Atlantic region and is followed by the Younger Dryas cold reversal indicated by abrupt decreases of MAT (from −2.2 to −5°C) and MAP (from 820 to 650 mm). The onset of the Holocene at about 11.5 cal ka BP is indicated by rises in reconstructed MAT (from −5 to about −0.3°C) and MAP (from 600 mm to 950 mm), which led to an increased supply of

weathered material and higher biological productivity. Between 5.0 and 3.0 cal ka BP, MAT increases to about 0.2°C and MAP rises to maximum values of about 1000 mm, followed by slightly decreasing MAT and MAP between 3.0 and 0 cal ka BP.

The biogeochemical parameters (total organic carbon (TOC), C/N, $\delta^{13}C_{org}$) and weathering indicators (e.g. the chemical index of alteration (CIA) and Sr/Ba) are directly (erosion of soils) or indirectly (changing provenance) related to moisture availability on the south-eastern TP and shows matching regional climate oscillations since the Late Glacial. In comparison to other Late-Glacial records from the TP, MAP reconstructions from Lake Naleng indicate wetter climate conditions in the south-eastern part of the TP and dryer conditions farther away from moisture sources.

1. Introduction

The Tibetan Plateau (TP) is the largest elevated landmass on Earth and triggers the onset of the monsoon circulation by increasing the insolation-driven thermal contrast between land and ocean (Prell and Kutzbach, 1992). Furthermore, the TP is very important for the water supply of billions of people, because it is the source area of the largest rivers in central Asia (Huang et al., 2011). Understanding regional natural landscape variability on the TP and adjacent areas will therefore provide insights into low-latitude climatic systems, and will enable better predictions of future climate change.

Because of its climatic impact on the atmospheric circulation system, the TP is a key region for palaeoclimate research. Most published palaeoclimate studies on the TP focus on the Holocene, and records including the Late Glacial are still rare (Herzschuh, 2006; Zhang and Mischke, 2009). A temporally and spatially extended data set of climate records from the Tibetan Plateau is useful for a regional assessment of the Late Glacial and Holocene climate and for a discussion of spatial heterogeneities of climate change on the TP (Shen et al., 2005; Mischke and Zhang, 2010). In this context, lake archives from the TP provide valuable information about environmental and climate change since the Late Glacial. However, different and interacting processes affect lake systems on the TP: hydrological and tectonic changes in the catchment, the existence of glaciers, or variations in precipitation, temperature and evaporation. Commonly used palaeolimnological proxies differ in the degree to which they are known to trace specific climatic parameters. For instance, individual proxies from the same site may suggest inconsistent climate reconstructions as they can reflect either local within-lake variations, regional variations or both (Wischnewski et al., 2011; Wang et al., 2014). Thus, validation procedures are needed to establish a reliable relationship between a climatic variable and a proxy indicator (IPCC, 2007).

Our objectives in this study were threefold. First, this study from Lake Naleng on the south-eastern TP presents quantitative palynological reconstructions for mean annual precipitation and temperature since 17.7 cal ka BP in comparison to other quantitative records from the eastern TP in order to determine the strength of, and the forcing mechanisms behind, climate oscillations in the Late Glacial and Holocene. Second, we present weathering indicator records (CIA, Sr/Ba, Y/Al, Al/Rb) to estimate the degree of weathering since the early Late Glacial. Third, we compared the palynological reconstructions with all newly available sedimentological and biogeochemical proxies (grain size, total organic carbon (TOC), C/N, $\delta^{13}C_{org}$) from Lake Naleng by principal component analyses to evaluate their traceability of temperature and precipitation and to estimate their usability as proxy indicators for local or regional environmental and climate variations.

2. Regional Setting

Lake Naleng (also referred as Lalong Cuo; 31.10°N, 99.75°E; Fig. 1) is situated in a glacial tongue basin, 4200 m above sea level (asl) on the south-eastern TP in the Shaluli Shan mountain range in the Sichuan Province of the People's Republic of China. The open freshwater lake (specific conductivity of 0.045 mS/cm) has a surface area of 1.7 km^2, a catchment area of 470 km^2 and a maximum water depth of 36.7 m (Kramer et al., 2010a, b, c). The lake has a Secchi depth of 2.9 m (determined 19.09.2003), a pH of 8.1 and a dissolved oxygen content of 6.9 mg/L, and is classified as mesotrophic water body (Kramer et a., 2010b). Today, the main inflow to Lake Naleng occurs through a major river channel on the northern side of the lake. Furthermore, several small streams from the surrounding mountains reach the lake. They originate from an elevation of approximately 4900 m asl (Kramer et al., 2010b). The outlet at the southern edge drains towards the Xinlong Plateau. Lake Naleng is currently not affected by glaciers but erratic boulders within the catchment area and marginal moraines near the lake-shore indicate its origin as glacially-formed basin (Graf et al., 2008). The Shaluli Shan mountain area includes both high-relief mountains and relatively low-relief upland landscapes. The regional bedrock geology is mainly composed of Triassic flysch sequences of the Songpan-Garze terrane and Triassic volcanic and sedimentary rocks, intruded by Jurassic plutons (Ouimet et al., 2010). However, the catchment area of the lake is composed of Miocene granite and granodiorite (Reid et al., 2005; Graf et al., 2008; Strasky et al., 2009). The main geomorphological units in this area are the Haizishan Plateau and the Xinlong Plateau (Fu et al., 2013a).

The study area is mainly influenced by the Indian summer monsoon, which transports warm and humid air masses from the Gulf of Bengal to the TP (Domrös and Peng, 1988). During winter, dry and cold air masses prevail in the investigation area, driven by the anticyclone over Mongolia. Mean January temperature is −3.9°C and mean July temperature is 14.3°C.

Most (90%) of the annual rainfall (560 mm) occurs during the summer monsoon season between May and October (measured at meteorological station Garzê, located about 80 km north-east of Lake Naleng, 31.62°N, 100.00°E, at 3522 m asl).

Lake Naleng is located at the upper tree-line and the vegetation between 3200 and 4400 m asl consists of conifer forests with *Abies squamata* and *Picea likiangensis*, and alpine meadows. The vegetation above the subalpine ecotone is mainly dominated by *Kobresia* species and *Polygonum sphaerostachyum* (Kramer et al., 2010b, c). Detailed information on the vegetation composition in the study area is given by Kramer et al. (2010a, b, c). The catchment area of the lake is used for grazing by yaks and sheep during summer.

Fig.1

3. Materials and Methods

3.1 Sediment core and dating

A 1781 cm long sediment core was recovered from the centre of Lake Naleng (Fig. 1) during a field campaign in February 2004 from 32 m water depth using an Uwitec (Niederreiter 60) piston corer system on the frozen lake surface (Kramer et al., 2010a). The age-depth model for the sediment core is based on AMS (accelerator mass spectrometry) radiocarbon dating of ten bulk organic carbon samples at the Leibniz Laboratory, Kiel. The humic acid fraction and leaching residue were analysed separately. The humic acid fraction was used for the construction of the age-depth model because this fraction is relatively insensitive to the re-deposition of older carbon or to the input of terrestrial material (Abbot and Stafford, 1996; Kramer et al., 2010b). The determined lake reservoir effect of 1500 cal a BP was calculated using two dated samples near the top of the sediment core and was subtracted from the original ^{14}C dating results (Kramer et al., 2010a, b). The reservoir effect is a common phenomenon on the TP and the determined age of about 1500 years corresponds to other lake studies on the TP (Yu et al., 2007; Hou et al., 2012; Mischke et al., 2013). Radiocarbon ages were calibrated using CALIB 5.0.1 (Stuiver and Reimer, 1993; Reimer et al., 2004). The sedimentation rate for the lower part of the sediment core (between 1800 and 950 cm) is about 2.2 mm/a. For the upper part (between 950 and 0 cm) the rate ranges between 1.3 to 0.6 mm/a. A detailed description of the age-depth model and the stratigraphy of the recovered sediment core from Lake Naleng is given by Kramer et al. (2010a).

3.2 Analytical methods

The laboratory analyses were conducted on 120 samples taken at intervals between 4 and 10 centimetres at the State Key Laboratory of Lanzhou Institute of Geology (Chinese Academy of Sciences). The determination of the carbonate content was conducted at 10-cm intervals using Chittick Apparatus. The procedure is based on the volumetric determination of carbon dioxide produced by the reaction of carbonates with 1N HCl (Dreimanis, 1962). Contents of carbon (C), TOC, and nitrogen (N) were determined on duplicate powdered samples using a Vario EL III (Elementar Analysensysteme GmbH, Hanau, Germany). For the determination of TOC, the sediment samples were pre-treated using 1N HCl to remove calcium carbonate.

Sub-samples were treated with 100% phosphoric for the determination of the organic carbon stable isotope composition ($\delta^{13}C_{org}$) using a Finnigan 252 mass spectrometer. The isotopic values are reported as delta per mil notation (δ, ‰) notation, relative to V-PDB. The analytical error is <0.3‰ for eight repeated measurements. Magnetic susceptibility measurements were performed at 6-cm intervals using a Bartington Instruments Ltd MS2 Magnetic Susceptibility Meter linked to an MS2B Dual Frequency Sensor (470 and 4700 Hz).

Element concentrations were determined by X-ray fluorescence spectroscopy (XRF) using a MagiX PW2403 at 4-cm intervals. The estimated accuracy is 1–2% for major elements and 5% for trace elements. The CIA was calculated to determine the weathering intensity in the catchment area. Baumann et al. (2014) showed that the CIA is the most suitable weathering index in permafrost ecosystems on the Tibetan Plateau. The CIA is defined as: $Al_2O_3/(Al_2O_3+CaO+Na_2O+K_2O)$ assuming that CaO comes mainly from silicates (Nesbitt and Young, 1982). This assumption applies to Lake Naleng due to the lack of calcareous rocks in the catchment area and the low carbonate content of the lake sediments (<1%). The element ratios Y/Al and Al/Rb are commonly used as physical weathering indicators (Krauskopf and Bird, 1995; Lucchini et al., 2003). Furthermore, the Sr/Ba ratio was used for weathering reconstructions, because Sr and Ba are included in feldspars of granites, and the Sr/Ba ratio traces the mobility of Sr relative to Ba (Liu et al., 1993).

Grain-size analyses were performed for the 0.02–2000 µm fraction using a Malvern Mastersizer 2000 laser granulometer at 4-cm sampling intervals. The samples were pre-treated using: (1) H_2O_2 to remove organic matter and soluble salts, (2) 10 % HCl to remove calcium carbonate, and (3) Na-hexametaphosphate to disperse aggregates.

A pollen-based calibration (transfer) function for eastern continental Asia from Cao et al. (2013) was applied to the pollen assemblages from the sediment core of Lake Naleng for the reconstruction of mean annual precipitation (MAP) and mean annual temperature (MAT) (Kramer et al., 2010a). A detailed description of the used dataset and the applied calibration function is given by Herzschuh et al. (2014).

Principal component analysis (PCA) was used and Pearson's correlation coefficient (r) calculated following the normalisation of the dataset using the OriginPro 9.0 software package. Missing data as a result of the different sampling resolutions between 4 and 10 cm intervals were interpolated using a linear interpolation algorithm before conducting PCA.

4. Results

4.1 General changes in TOC, C/N ratio, $\delta^{13}C_{org}$, MAP and MAT

The TOC contents generally range between 0.2 and 12% (Fig. 2). TOC is low below 950 cm (before 14.5 cal ka BP) and increases to 11% at 700 cm (8.3 cal ka BP), followed by fluctuating values between 6-12% (Fig. 2). The C/N ratio generally ranges between 2 and 17 and shows a similar pattern as TOC (Fig. 2). Below 1000 cm (before 14.0 cal ka BP) the C/N ratio is mostly below 8 rises to 13 at 1050 cm (14.3 cal ka BP). From 1050 cm to 0 cm (between 14.0 to 0.0 cal ka BP) the C/N ratio range between 10 and 17.

The $\delta^{13}C_{org}$ values of the sediment core range between −31 and −26‰ and show an inverse pattern to TOC and the C/N ratio (Fig. 2). Below 1000 cm (14.5 cal ka BP) the values range between −28.5 and −25‰. From 1000 cm to the top (between 14.5 to 0 cal ka BP) the $\delta^{13}C_{org}$ values range between −29.5to −27.5‰.

The pollen-based reconstructed MAP ranges between 371 and 973 mm (Fig. 2). Below 1000 cm (before 14.5 cal ka BP) the values are relatively low and range between 400 and 580 mm. From 1000 to 730 cm (14.5 to 8.5 cal ka BP) the values rise to a maximum of 973 mm and slightly decrease to 780 mm at about 600 cm (7.5 cal ka BP). Between 600 and 0 cm (since 7.5 cal ka BP), MAP remains relatively high and range between 820 and 960 mm.

Reconstructed MAT ranges between −5.1 and 0.3°C (Fig. 2). Below 820 cm (before 11.0 cal ka BP) MAT is slightly decrease from about −2.0 to −5.0°C. From about 820 to 700 cm (14.3 to about 8.5 cal ka BP) the values rise to 0.2°C and show a subsequent decreasing trend between 700 and about 520 cm (8.5 to 6.8 cal ka BP) to a minimum value of −5.1°C. From 520 to 0 cm (6.8 to 0.0 cal ka BP) MAT increases to a maximum value of 0.3°C.

Fig. 2.

4.2 General changes in grain-size, weathering indicators, magnetic susceptibility, and element concentrations and ratios

The median grain size ranges between 4 and 24 µm (Fig. 3). Grain-size variations are large in the lowermost part between 1780 and 1400 cm (between 17.7 and 16.4 cal ka BP). The median grain size ranges between 4 and 16 µm in the section between 1400 and 1000 cm (16.2 to 14.3 cal ka BP). Above, the median varies in a relatively narrow range between 8 and 12 µm.

In the lowermost part of the sediment core between 1780 and 1600 cm (17.7 to 17.0 cal ka BP) the clay content (<2 µm) ranges between 10 and 25%, silt content (2–63 µm) ranges between 72 and 90%, and the sand content (>63 µm) ranges between 0 and 25% (Fig. 3). Between 1600 and 1450 cm (between 17.0 and 16.6 cal ka BP) the clay content shows high variability and rises at 1500 cm (16.8 cal ka BP) to a maximum value of 27%. Silt content ranges between 60 and 96% and drops at 1650 cm (16.6 cal ka BP) to a minimum of 40%. The sand content is relatively low between 0 and 10% and rises at 1450 cm (16.6 cal ka BP) to a maximum value of 58%. From 1450 to 1000 cm (16.6 to 14.3 cal ka BP) the clay content shows an increase from 4 to about 22%, whereas silt fluctuates between 60 and 90% and sand between 0 and 22%. Between 1000 and 800 cm (between 14.3 and 10.1 cal ka BP) the clay content decreases from 22% to 5% whereas the silt content increases from 80 to 92%. Sand content ranges between 0 and 3% interrupted by a relatively high value of 20% at about 890 cm (11.1 cal ka BP). From 800 to 0 cm (10.1 to 0 cal ka BP) the grain-size fraction is relatively stable. Clay content ranges between 10 and 15%, silt ranges mainly between 80 and 90%, and sand ranges between 2 and 20%.

Below 1000 cm (before 14.3 cal ka BP) all weathering indicators show similar patterns with relatively low values (Fig. 4), except Al/Rb. Between 1000 and 0 cm (between 14.3 and 0.0 cal ka BP) increase and are remain high until the top, except Y/Al and Al/Rb, which show a variable pattern.

The oxide compounds Fe_2O_3 and MgO show a similar uniform pattern with relatively stable values below 1000 cm (before 14.3 cal ka BP), interrupted by a sharp increase at 1450 cm (16.6 cal ka BP), followed by an increase from 1000 to about 600 cm (between 14.3 and 7.3 cal ka BP) and relatively high concentrations afterwards (Fig. 5). SiO_2, Al_2O_3, CaO, Na_2O, and K_2O show uniform patterns with relatively high values below 1000 cm (before 14.3 cal ka BP) interrupted by a sharp decrease at 1450 cm (16.6 cal ka BP). From 1000 to about 600 cm (14.3 to 7.3 cal ka BP) the concentrations abruptly decrease followed by relatively low values until the top of the sediment core.

Below 1000 cm (before 14.3 cal ka BP) Mg/Ca ratios show low values (Fig. 5). Highest Mg/Ca values occur between 1000 and 800 cm (between 14.3 and 10.1 cal ka BP). Between 800 and 0 cm (between 10.1 and 0 cal ka BP) Mg/Ca ratios show a strong variability and slightly decrease.

The low frequency magnetic susceptibility (χ_{LF}) ranges between 0.8 and 3.0 x $10^{-7} m^3 kg^{-1}$ (Fig.4). Below 1000 cm (before 14.3 cal ka BP) the χ_{LF} values are relatively low and range between 1.2 and 1.8 x $10^{-7}m^3$ kg^{-1}, interrupted by an abrupt rise at 1450 cm (16.8 cal ka BP). From 1000 to 900 cm (14.3 to 12.0 cal ka BP) the values increase to around 2.0 x $10^{-7}m^3$ kg^{-1} and remain relatively high between 900 to 300 cm (between 12.0 and 2.8 cal ka BP). Above, the values decrease to a low level of about 1.0 x $10^{-7}m^3$ kg^{-1}.

Fig. 3-5

4.3 PCA of sedimentological, geochemical, and magnetic properties and transfer-function derived MAP and MAT

The PCA biplot of Figure 6 shows the interrelationships between different variables analysed for the Lake Naleng record. The first two eigenvectors (PCA 1 and PCA 2) account for 85.8% of the total variance. PCA 1 accounts for 53.1% of the total variance and is mainly controlled by MAP, TOC, C/N, Fe_2O_3, Al/Rb, CIA, and Sr/Ba at the positive end and Na_2O_3, CaO, K_2O, SiO_2 and $\delta^{13}C_{org}$ at the negative end (Fig. 6). PCA 2 accounts for 32.7% of the total variance and is mainly controlled by χ_{LF}, MgO, and Y/Al at the positive end and MAT and Mean grain size at the negative end. The correlation between pollen-related and non-pollen data is highest for MAP and TOC (r=0.95), MAP and Sr/Ba ratios (r=0.91), and MAP and C/N ratios (r=0.86, Fig. 6). Highly anti-correlated are SiO_2 and Fe_2O_3 (r=–0.88) and SiO_2 and CIA (r=–0.75). The low significance of the positions of the grain-size fractions in the biplot is indicated by short arrows (Fig. 6).

Fig. 6

5. Discussion

5.1 Development of Lake Naleng since the Late Glacial

5.1.1 Late Glacial (1780–900 cm, 17.5–11.5 cal ka BP)

Pollen-based reconstructions of MAP (around 600 mm) and MAT (about −3°C) indicate a relatively dry and cold climate during the Late Glacial. C/N values mainly below 10 suggest that the remains of aquatic organisms predominate in the Naleng Co record and point to a very low input of terrestrial plant material (Cummins and Klug 1979; Meyers 1994; Meyers and Teranes 2001. According to Kasper et al. (2015), Shen et al. (2005) relatively low TOC values indicate a low biological productivity within the lake during the Late Glacial.

Relatively high $\delta^{13}C_{org}$ values (>−25‰) during the Late Glacial suggest that the bulk of the organic matter derived from the growth of macrophytes which was already described by Kramer et al. (2010b). Pollen from macrophytes such as *Hippuris, Myriophyllum* and *Potamogeton*, and high percentages of algae (*Botryococcus, Spirogyra and Pediastrum*) were recorded (Kramer et al., 2010b).

Grain-size variations within the lowermost sediments suggest alternating modes of detrital sediment supply. The relatively high clay content of about 12–20% and the high concentrations of Al_2O_3, SiO_2, Na_2O and K_2O at about 17.5 and 15.5 cal ka BP are possibly related to the input of fine-grained detrital material originating from glacial erosion. Rock flour produced by glacial abrasion has a significant proportion of clay to silt-sized particles (Fenn and Gomez, 1989; Benson et al., 1998; Rosenbaum and Reynolds, 2004) and is typical for unaltered detrital sediments in a partly glaciated, alpine catchment (Zhang and Mischke, 2009). The assumption of the influx of unaltered rock flour is supported by relatively low weathering indicator values and by ^{10}Be age determinations from inner, middle, lateral, and outer end moraines near Lake Naleng which suggest that the upper catchment was covered by glaciers during the Late Glacial (Strasky et al., 2009; Fu et al., 2013a). The calculated and erosion-corrected exposure ages for moraines in the outlet area of Lake Naleng range between 21.5 and 17.5 ka BP and represent the period of basin formation by an advancing glacier during the global Last Glacial Maximum (LGM; Strasky et al., 2009, Fig. 1). We therefore assume, that Lake Naleng received glacially-derived unaltered detrital sediments from local sources during the Late Glacial.

The climate conditions changed abruptly during the second half of the Late Glacial. Increasing MAT (from –4 to –2.2°C) and MAP (from 500 mm to 820 mm) between 14.5 and 13.0 cal ka BP indicate a climate amelioration. This time interval probably corresponds to the Bølling/Allerød (B/A) warming period in the North Atlantic region (Kramer et al., 2010b). Based on the observed temperature gradient on the TP of 0.5°C per 100 m difference in elevation (Böhner, 1994), today's estimated MAT is 1.6°C at Lake Naleng (Kramer et al., 2010c). Increasing TOC contents also reflect a climatic change to warmer and moister conditions and point to amplified lake productivity as a consequence of the climate amelioration.

The increase of MAP correlates with increasing CIA values implying that CIA is linked to the moisture availability in the study area. Baumann et al. (2014) showed that weathering processes on the TP are directly linked to climatic gradients and pedogenesis and reflected by CIA. High Mg/Ca ratios after 14.5 cal ka BP may also indicate the influence of pedogenic minerals (Chamley, 1989). The temporal correlation of MAP and CIA with the beginning of the B/A possibly indicates the formation and erosion of soils. Weakly developed polygenetically formed soils were found on slopes and terraces and occur often in topographic depressions close to rivers and lakes (Kaiser, 2004; Kaiser et al., 2007). The instability of the soil substrates is related to intense precipitation during summer months leading to fluvial erosion and alluvial accumulation (Baumann et al., 2014). According to Shao and Yang (2012), the temporal correlation of weathering indicators and MAP is possibly linked to a changing provenance in relation to the shift of the precipitation zone with the onset of moisture climate conditions. A changing provenance can possibly be inferred by rising Y/Al, Al/Rb, Sr/Ba ratios, χ_{LF} values and simultaneously decreasing Al_2O_3, SiO_2, Na_2O and K_2O concentrations, which indicate a different composition of the sediment supply compared to the first half of the Late Glacial. However, a changed provenance within the catchment is rather unlikely, because the catchment area of Lake Naleng is very small and characterized by granite or granodiorite rocks. Possibly due to the increasing precipitation the provenance from discharging streams which orginate on a elevation of 4900 m was changed and led to a changed sediment supply.

We therefore assume that the weathering dataset of our record indicate the erosional input of weathering products, which are directly (erosion of soils) or indirectly (changing provenance) linked to changes of MAT and MAP. Furthermore decreasing clay contents suggests a decreasing influence of glaciers in the area. This assumption correlates with the start of the deglaciation with the onset of the B/A period at about 14.7 ka BP (Strasky et al., 2009).

From 13.0 to 11.5 cal ka BP an abrupt decrease in MAT (from −2.2 to −5°C) and MAP (from 820 to 650 mm) indicates cooler and dryer climate conditions, which is probably associated with the North Atlantic Younger Dryas (YD) period (Kramer et al., 2010c). This climate deterioration is also reflected in the non-pollen dataset of Lake Naleng by decreasing TOC resulting from a decrease of biological productivity. Given the temperature gradient discussed above, the reconstructed MAT suggests that during the YD temperatures were ~6°C colder than today and about 2°C colder than in the first part of the Late Glacial.

5.1.2 Early to mid Holocene (900–280 cm, 11.5–5.0 cal ka BP)

The onset of the Holocene at Lake Naleng is indicated by a rise in MAT (from −5 to about −0.3°C) and MAP (from 600 to 950 mm). This change is also reflected by incresing TOC and decreasing $\delta^{13}C_{org}$ values which suggest an increase in biological productivity. A change in the origin of organic matter to almost exclusively phytoplankton within the lake was already indicated by the palynological analysis (Kramer et al., 2010b).

All weathering indicators suggest a relatively high input of weathering material, which is probably directly (erosion of soils) or indirectly (changes of the provenance) related to the increased moisture availability during the start of the Holocene. This time period was characterized by alpine meadow and montane forest at Lake Naleng (Kramer et al., 2010b). Possibly the increasing supply of weathered material into the lake was triggered by increasing fluvial erosion due to intense precipitation, which caused a instability of soils in depressions around the lake (Baumann et al., 2014).

Lake systems on the TP are known to be sensitive to moisture changes. The early–mid Holocene time interval was characterized by high lake levels indicated by palaeoshorelines around the lakes (Liu et al., 2013) and fine-grained material settling out within lake basins (Opitz et al., 2012). Although the climate situation in the study area was characterized by relatively high MAP values during the early to mid Holocene, the clay-size fraction shows no distinct variations at Lake Naleng, which suggests relatively stable lake levels. Indications for a higher lake levels like palaeoshorelines around the lake were not found during the field campaign. The lack of indications for higher lake levels supports the assumption that Lake Naleng was an open-basin lake as today at least since the early Holocene.

MAP and MAT values decreased between 8.3 and 7.3 cal ka BP. MAT dropped to −5°C and MAP to 800 mm during this period indicating climatic deterioration. When allowing for dating uncertainty, this cold and dry period is possibly related to the North Atlantic 8.2 ka event (Kramer et al., 2010c). The cold-dry event is possibly also reflected in the non-pollen data of Lake Naleng. A abrupt drop of TOC corresponds to the MAP and MAT reductions and indicates decreasing biological productivity at about 7.3 cal ka BP. However, relatively stable low $\delta^{13}C_{org}$ values indicate the dominance of planktonic algal remains.

During the cold-dry period between 8.3 and 7.3 cal ka BP decreasing Y/Al and χ_{LF} values, increasing SiO_2 concentrations and coarser material suggest a different composition of the terrestrial sediment input. Possibly, the changing composition can be explained by a more intense aeolian sediment supply into the lake due to drier and colder climate conditions. An increasing input of aeolian material at about 8.2 ka BP is also described for Genggahai Lake on the north-eastern TP (Li et al., 2015).

The abrupt climate deterioration after 8.2 cal ka BP was followed by climate amelioration indicated by MAP values above 950 mm and increasing MAT, culminating at about 5.5 cal ka BP and reaching values above 0°C for the first time. The climate amelioration is also reflected by high TOC contents, which suggest a rise of biological productivity. C/N ratios of around 12 suggest input of terrestrial plant material in addition to aquatic material due to the dense vegetation cover within the catchment. Very low $\delta^{13}C_{org}$ values indicate a predominating origin of organic matter from planktonic production. The grain-size distributions of the sediment record show only minor changes and suggest enhanced stable open-lake conditions.

Mostly all weathering indicators and the χ_{LF} values mirror the increasing moisture availability and show highest values during the mid-Holocene. The increasing input of weathered material suggests that the sediment supply into Lake Naleng was similar to the end of the Late Glacial and the early Holocene directly or indirectly controlled by the increasing precipitation.

Another dramatic climatic change to cooler and dryer conditions is documented at about 5.0 cal ka BP by the abrupt decline of MAT from around 0°C to about −4°C, which was resulting in a downward shift of the treeline (Kramer et al., 2010a). The abrupt cooling occurred probably within a few hundred years and is also seen in an abrupt decline of TOC and $\delta^{13}C_{org}$ values.

5.1.3 Late Holocene (280–0 cm, 5.0–0.0 cal ka BP)

MAT increased to about 0.2°C and MAP rose to maximum values of about 1000 mm after 5.0 cal ka BP. Increasing TOC also documents this climate period during the early stage of the late Holocene and decreasing C/N ratios point to a slight decrease in terrestrial matter contribution. The increasing $\delta^{13}C_{org}$ values point to a simultaneously decreasing relative contribution of planktonic algae to the lake sediments.

Based on the Lake Naleng pollen record, forest began to decline after 3.4 cal kyr BP. Frequently found grazing indicators such as *Sanguisorba, Rumex,* and Apiaceae are possibly a result of human impact (Kramer et al., 2010c). The change in vegetation correlates with the abrupt decline of χ_{LF} values and Y/Al ratios from about 3.0 to 1.0 cal ka BP, which probably reflects a slowing down of the weathering processes. Since 1.0 ka BP increasing χ_{LF} values, Al/Rb and Y/Al ratios indicate re-initiated erosion processes. Possibly, human impact on the vegetation in the catchment of the lake resulted to a *meadow* and *shrub* vegetation (Kramer et al., 2010c), which possibly caused an increased supply of erosional weathering products. Alpine meadow soil is an important ecosystem component on the TP and degradations due to global climate change, overgrazing, human activities and rodents have enormous influence on physical and chemical soil properties (Zeng et al., 2013).

5.2 Comparison of pollen-based inferences to the non-pollen record from Lake Naleng

The high correlation coefficients of MAP and TOC (positively correlated) and MAP and $\delta^{13}C_{org}$ (inversely correlated) of PCA 1 indicate that TOC and $\delta^{13}C_{org}$ are strongly related to the moisture availability on the south-eastern TP (Fig. 6). The correlation between MAP and TOC and the low correlation between MAP and MAT suggest that the amount of organic matter is probably linked to the availability of nutrients via fluvial input, which was also assumed by Kramer et al. (2010b). In addition to the biochemical proxies, the weathering indicators Sr/Ba, CIA and Al/Rb are highly correlated with the MAP record (PCA 1, Fig. 6) indicating directly (development of soils) or indirectly (changing provenance) the moisture availability in the area starting at about 14.5 cal ka BP. The increasing alteration pattern is also reflected by a high correlation between CIA and Fe concentrations (PCA 1, r=0.89), which possibly suggests changes in the redox system during the development of soils (Figs. 4, 6).

In contrast to the biogeochemical or weathering proxies, the grain-size record does not show high correlation values with MAP or MAT (Fig. 3). The relatively low statistical significance probably results from the open lake system since at least the end of the Late Glacial and implies that the grain-size record of Lake Naleng only reflects changes within the lake setting and is not directly linked to moisture changes. χ_{LF} values and Y/Al ratios show no distinct correlation to MAP or MAT but a relatively high correlation to each other, which suggests that both proxies are related to similar processes.

Excluding the grain-size data, the non-pollen biogeochemical parameters (TOC, C/N, $\delta^{13}C_{org}$) and weathering indicators (e.g. CIA and Sr/Ba) from the Lake Naleng record accord well with the pollen-based reconstructions of MAP and provide supporting evidence for regional climate oscillations on the south-eastern part of the TP. Short-term oscillations are especially well reflected by the biogeochemical record.

The results of sedimentological, biogeochemical, and geochemical analyses in comparison to reconstructed MAT and MAP indicate that the multi-proxy dataset from Lake Naleng captures both local changes and regional climate signals.

The comparison of pollen and non-pollen data of the Lake Naleng record shows that a combination of sedimentological, biogeochemical, and palaeoecological multi-proxy datasets is ultimately necessary to separate local geological and geomorphological signals from regional and hemispheric climate signals. Furthermore, the findings suggest that for a plateau-wide climatic reconstruction on the basis of different lake archives, similar related proxy records have to be considered.

5.3 Climatic implications and comparison with other records from the eastern TP

5.3.1 Late Glacial

Lake Naleng was affected by the direct influence of glaciers between 17.7 and 14.6 cal ka BP. ^{10}Be exposure age determinations of nine erratic boulders from two inner end moraines suggest glacier expansions in the study area between 22.2 to 17.6 BP, implying that a glacier covered most of the catchment area including the modern lake basin (Strasky et al., 2009; Fu et al., 2013a). The early Late Glacial age of the basal lake sediments of the recovered core corresponds to the dated glacier advances in the LGM and later on. A similar lake history on the south-eastern TP with the formation of the lake basin through a glacier advance in the LGM and a subsequently high supply of glacier meltwater during the Late Glacial was also proposed for Lake Ximencuo 280 km north-east of Lake Naleng (Zhang and Mischke, 2009).

Reconstructed MAP and MAT at Lake Naleng point to cold and relatively dry conditions with relatively low precipitation rates (400–600 mm) between 17.5 and 14.6 cal ka BP in comparison to today's climate. These reconstructed cold and relatively dry conditions correspond well with other palaeoclimate records from the eastern TP (Herzschuh et al., 2009; 2014).

The reconstructed MAP of 500–600 mm between 17.5 and 14.6 cal ka BP is slightly higher than pollen-based MAP at Lake Yidun (400–500 mm; Shen et al., 2006; Wang et al., 2013), Lake Kuhai (300–400 mm; Wischnewski et al., 2011; Wang et al., 2013), Lake Donggi Cona (200–300 mm; Wang et al, 2013) and Lake Luanhaizi (200–300 mm; Herzschuh et al., 2010; Wang et al., 2013) on the eastern TP. The spatial pattern of decreasing MAP towards the north suggests that climate conditions on the south-eastern TP were slightly wetter than on the north-eastern TP during the Late Glacial.

Relatively moisture climate (MAP at about 800 mm) conditions occurred at the lake between 14.0 and 13.0 cal ka BP, which correlates with the B/A warming period in the North Atlantic region. The B/A warming is also observed in records from Hulu and Dongge caves in eastern China (Dykoski et al., 2005; Wang et al., 2008) and is probably associated with the strengthening of the summer monsoon system and high summer precipitation rates (Herzschuh et al., 2005).

In contrast to the B/A, the following interval between 13.0 to 11.5 cal ka BP is characterized by cooler and dryer conditions indicated by pollen and non-pollen data of the Lake Naleng record. This period is probably associated with the North Atlantic YD cold reversal (Kramer et al., 2010c). The widespread climate event was probably forced through a strengthened westerly circulation in central Europe (Mischke et al., 2010). The YD was inferred from several paleoclimate studies based on lake records from the Tibetan Plateau: e.g. Lake Qinghai (Ji et al., 2005; Shen et al., 2005) or Lake Donggi Cona (Opitz et al., 2012). However, MAP reconstructions from Lake Naleng indicate precipitation rates of about 700 mm during the YD period, which is slightly above precipitation reconstructions for other sites on the eastern TP (Wang et al., 2013). Following the discussion above, this palaeo-precipitation pattern implies that the south-eastern TP experienced more humid conditions during the cold and dry YD in contrast to the north-eastern part of the TP. The cold and dry YD period possibly corresponds to reconstructed glacier advances near Kanding, in the Daxue Mountains (about 165 km farther east), between 14.3 and 12.0 ka BP (Strasky et al., 2007).

5.3.2 Early to mid Holocene

The beginning of the early Holocene at Lake Naleng about 11.5 cal ka BP was associated with increasing temperatures and precipitation rates culminating at about 9.0 cal ka BP. The climate amelioration was probably associated with a strengthened summer monsoon (Kramer et al., 2010c) triggered by the summer insolation maximum (An et al., 2000; Chen et al., 2008). The warming trend during the early and mid Holocene was also identified at other places on the TP (An et al., 2000) and is known as a high-lake level period. Lakes on the Tibetan Plateau were several times larger during the early–mid Holocene than today according to their relict shorelines (Avouac et al., 1996; Kong et al., 2011; Liu et al., 2013a), which is also documented for lakes and thermokarst basins on the north-eastern TP (Opitz et al., 2012, 2013).

MAP reconstructions at Lake Naleng indicate higher precipitation rates in comparison to other lakes on the north-eastern TP – Lake Yidun (500–600 mm; Shen et al., 2006; Wang et al., 2013), Lake Kuhai (400–450 mm; Wischnewski et al., 2011; Wang et al., 2013), Lake Donggi Cona (300–350 mm; Wang et al., 2013) and Lake Luanhaizi (400–500 mm; Herzschuh et al., 2010; Wang et al., 2013). The northward decrease of MAP is possibly related to spatial climate differences and diminished moisture availability by a weaker influence of the Asian monsoonal system towards the more continental interior of the TP. However, further investigations of palaeoclimate archives are required to assess spatial differences of MAP during the early to mid Holocene.

The recorded cold period between 8.3 and 7.5 cal ka BP at Lake Naleng correlates with monsoonal signals derived from the Guliya ice-core and the Dongge cave speleothem records (Thompson, 2000; Dykoski et al., 2005) and probably represents the 8.2 ka event. This cold and dry event is reported from several sites on the TP: lakes Qinghai at 8.2 ka, Ximencuo at 8.3 ka BP, Koucha at 8.5 ka BP, Zigetang during 8.7–8.3 ka BP, Cuoe during 8.8–8.6 ka BP, and from the Hongyuan peat during 8.3–7.8 ka BP (Shen et al., 2005; Herzschuh et al., 2006; Wu et al., 2006; Yu et al., 2006; Mischke et al., 2008; Zhang and Mischke, 2009). Because of the temporal correlation of the inferred climate reversal around 8.2 ka BP it has already been assumed that this cold event is the result of a linkage between the North Atlantic realm and the Tibetan Plateau by a simultaneously acting trigger mechanism (Zhang and Mischke 2009; Liu et al., 2013a).

5.3.3 Late Holocene

After the climate amelioration and its culmination at about 5.5 cal ka BP, another cold period was inferred from the pollen and non-pollen Lake Naleng records. According to Morrill et al. (2003), this cold event which was recorded between 5.0 and 4.5 cal ka BP was apparently widespread across central Asia and was also inferred from Lake Donggi Cona and adjacent thermokarst lakes (Opitz et al., 2012, 2013), Lake Ximencuo (Zhang and Mischke, 2009) and Lake Bangong (Van Campo and Gasse, 1993; Gasse et al., 1996) on the TP. Within dating uncertainty, this cold event is also referred to as the “4.2 event” (Yu et al., 2000, 2009). Cooling after 5.0 cal ka BP can be regarded as a widespread climate event in eastern and central to southern Asia (Yu et al., 2009; Mischke and Zhang, 2010), and the Indian subcontinent (Staubwasser et al., 2003). This incipient cold period might have resulted in significant aridification and the collapse of ‘Old World’ cultures (Yu et al., 2000) and ancient civilizations in central China (deMenocal, 2001; Wu and Liu, 2004; An et al., 2005; Shao et al., 2006; Mischke and Zhang, 2010). A possible explanation for the cold and dry period beginning at about 5.0 cal ka BP is the insolation-driven threshold-type weakening of the summer monsoon (Berger and Loutre, 1991; Overpeck et al., 1996; Wu and Liu, 2004).

From 5.0 to 0.0 cal ka BP Lake Naleng was similar to the early-mid Holocene affected relatively high reconstructed MAT (-2-2°C) and MAP (around 800 mm). Reconstructed MAP from Lake Yidun (around 700 mm; Shen et al., 2006; Wang et al., 2013), Lake Kuhai (400–450 mm; Wischnewski et al., 2011; Wang et al., 2013), Lake Donggi Cona (around 300 mm; Wang et al., 2013) and Lake Luanhaizi (around 300 mm; Herzschuh et al., 2010; Wang et al., 2013) indicate a trend towards dryer conditions from south to north on the eastern part of the TP. This trend can be probably explained by the diminishing influence of the Asian monsoon in the northern part of the TP due to the increased continentality. However, further multiproxy studies are needed to decipher the complex relationships of Holocene moisture and temperature change on the eastern TP and its impact on the environment.

6. Conclusions

Our record from Lake Naleng from the south-eastern TP shows that during the Late Glacial from 17.7 to 14.0 cal ka BP the lake was affected by relatively cold and dry climate conditions (MAP: about 600 mm and MAT about −3°C) and low biological productivity. Further the supply of unaltered fine-grained material due to the supply of glacier milk indicates a sensitive glacier response.

The climate changed abruptly during the second half of the Late Glacial. MAT and MAP increased (from −4 to −2.2°C and from 500 mm to 820 mm, respectively) between 14.0 and 13.0 cal ka BP and led to generally warmer and wetter climate conditions. This time interval can be correlated to the Bølling/Allerød (B/A) warming period in the North Atlantic region and is followed by the Younger Dryas cold reversal indicated by abrupt decreases of MAT (from −2.2 to −5°C) and MAP (from 820 to 650 mm).

The onset of the Holocene at about 11.5 cal ka BP is indicated by rises in reconstructed MAT (from −5 to about −0.3°C) and MAP (from 600 mm to 950 mm), higher biological productivity and the increased supply of weathered material. MAT increased to about 0.2°C and MAP rose to maximum values of about 1000 mm between 5.0 and 3.0 cal ka BP, followed by slightly decreasing MAT and MAP between 3.0 and 0 cal ka BP. In comparison to other Late Glacial records from the eastern TP, MAP reconstructions from Lake Naleng indicate wetter climate conditions in the south-eastern part of the TP and dryer conditions farther away from moisture sources.

Our comparison of a newly available sedimentological and biogeochemical record with palynological reconstructions of variations in MAP and MAT from Lake Naleng shows that the biogeochemical dataset (TOC, C/N, $\delta^{13}C_{org}$) is strongly related to moisture availability and shows concomitant evidence for regional climate oscillations on the south-eastern part of the TP. The weathering indicators (e.g. CIA and Sr/Ba) are highly correlated to MAP and reflect general moisture changes on the TP since the Late Glacial. The input of weathered material is either related to pedogenesis or linked to different supply areas in relation to changed climate conditions.

Our study demonstrates how a palaeoenvironmental study can benefit from methodologically different parameters. The study has shown that a multi-proxy record based on sedimentological, biogeochemical, and palynological data is ultimately necessary to reconstruct the lake development, environmental conditions and climatic changes. However, further investigation on erosional processes in relation to vegetation density is necessary to gain deeper insights into the landscape development on the south-eastern TP since the Late Glacial. Furthermore, we were not able to decipher the human impact on the catchment (e.g vegetation density) sufficiently during the late Holocene. Thus, the investigation of effects of human activity like overgrazing on the sensitive landscape on the TP is still an important challenge for future palaeoenvironmental studies.

Acknowledgements

We thank Emi Ito and Shiyong Yu for reviewing the manuscript and for their very helpful comments. We further thank Qili Yang, Huaming Shang and Yanbin Lei for help during fieldwork. This work was supported by the Deutsche Forschungsgemeinschaft (DFG He

3622/3-1 and Mi 730/1-1). Stephan Opitz is grateful to the University of Potsdam for a graduate fellowship.

References

Abbott, M.B., Stafford, T.W., 1996. Radiocarbon geochemistry of modern and ancient arctic lake systems, Baffin Island, Canada. Quaternary Research 45, 300–311.

Avouac, J.P., Bourjot, L., Dobremez, J.F., 1996. Paleoclimatic interpretation of a topographic profile across middle Holocene regressive shorelines of Longmu Co (western Tibet). Paleogeography, Paleoclimatology, Paleoecology 120, 93– 104.

Baumann, F., Schmidt, K., Dörfer, C., He, J. S., Scholten, T., Kühn, P., 2014. Pedogenesis, permafrost, substrate and topography: Plot and landscape scale interrelations of weathering processes on the central-eastern Tibetan Plateau. Geoderma 226-227, 300-316.

Benson, L.V., May, H.M., Antweiler, R.C., Brinton, T.I., Kashgarian, M., Smoot, J.P., Lund, S., 1998. Continuous lake-sediment records of glaciation in the Sierra Nevada between 52,600 and 12,500 ^{14}C yr BP. Quaternary Research 50, 113–127.

Berger A., Loutre M.F., 1991. Insolation values for the climate of the last 10 million years. Quaternary Science Reviews 10, 297–317.

Birks, H.H., Birks, H.J.B., 2006. Multi-proxy studies in palaeolimnology. Vegetation History and Archaeobotany 15, 235-51.

Böhner, J., 1994. Circulation and representativeness of precipitation and air temperature in the southeast of the Qinghai–Xizang Plateau. GeoJournal 34, 55–66.

Cao, X., Ni, J., Herzschuh, U., Wang, Y., Zhao, Y., 2013. A late Quaternary pollen dataset from eastern continental Asia for vegetation and climate reconstructions: set up and evaluation. Review of Palaeobotany and Palynology 194, 21-37.

Chamley, H., 1989. Clay Sedimentology. Springer, Berlin, 623 pp.

Chen, F.H., Yu, Z.C., Yang, M.L., Ito, E., Wang, S.M., Madsen, D.B., Huang, X.Z., Zhao, Y., Sato, T., Birks, H.J.B., Boomer, I., Chen, J.H., An, C.B., Wünnemann, B., 2008. Holocene moisture evolution in arid central Asia and its out-of-phase relationship with Asian monsoon history. Quaternary Science Reviews 27, 351–364.

Cummins, K.W., Klug, M.J., 1979. Feeding ecology of stream invertebrates. Annual Review of Ecology, Evolution and Systematics 10, 147–172.

deMenocal, P.B., 2001. Cultural responses to climate change during the last late Holocene. Science 292, 667–673.

Domrös, M., Peng, G., 1988. The climate of China. Springer, Berlin, Heidelberg, 361pp.

Dreimanis, A., 1962. Quantitative gasometric determinations of calcite and dolomite by using Chittick apparatus. Journal of Sedimentary Petrology 32, 520–529.

Dykoski, C., Edwards, R., Cheng, H., Yuan, D., Cai, Y., Zhang, M., Lin, Y., 2005. A high-resolution, absolute-dated Holocene and deglacial Asian monsoon record from Dongge Cave, China. Earth and Planetary Science Letters 233, 71-86.

Fenn, C.R., Gomez, B., 1989. Particle size analysis of the sediment suspended in a proglacial stream: Glacier de Tsidjiore Nouve, Switzerland. Hydrological Processes 3, 123–135.

Fu, P., Stroeven, A.P., Harbor, J.M., Hättestrand, C., Heyman, J., Caffee, M., Zhou, L.P., 2013a. Paleoglaciations of the Shaluli Shan, southeastern Tibetan Plateau. Quaternary Science Reviews 64, 121-135.

Fu, P., Harbor, J.M., Stroeven, A.P., Hättestrand, C., Heyman, J., Zhou, L.P., 2013b. Glacial geomorphology and paleoglaciation patterns in Shaluli Shan, the southeastern Tibetan Plateau - evidence for polythermal ice cap glaciation. Geomorphology 182, 66-78.

Gasse, F., Fontes, J.C., Van Campo, E., Wei, K., 1996. Holocene environmental changes in Lake Bangong basin (Western Tibet). Part 4: discussion and conclusion. Palaeogeography, Palaeoclimatology, Palaeoecology 120, 79–92.

Graf, A.A., Strasky, S., Zhao, Z.Z., Akçar, N., Ivy-Ochs, S., Kubik, P.W., Christl, M., Kasper, H.U., Wieler, R., Schlüchter, C., 2008. Glacier extension on the eastern Tibetan Plateau in response to MIS 2 cooling, with a contribution to ^{10}Be and ^{21}Ne methodology. In: Strasky, S.

(Ed.), Glacial Response to Global Climate Changes: Cosmogenic Nuclide Chronologies from High and Low Latitudes (PhD thesis, ETH Zürich).

Hannon, G.H., Gaillard, M.J., 1997. The plant-macrofossil record of past lake-level changes. Journal of Paleolimnology 18, 15–28.

Herzschuh, U., Zhang, C., Mischke, S., Herzschuh, R., Mohammadi, F., Mingram, B., Kürschner, H., Riedel, F., 2005. A late Quaternary lake record from the Qilian Mountains (NW China), evolution of the primary production and the water depth reconstructed from macrofossil, pollen, biomarker, and isotope data. Global and Planetary Change 46, 361–379.

Herzschuh, U., 2006. Palaeo-moisture evolution at the margins of the Asian monsoon during the last 50 ka. Quaternary Science Reviews 25, 163–178.

Herzschuh, U., Winter, K., Wünnemann, B., Li, S., 2006. A general cooling trend on the central Tibetan Plateau throughout the Holocene recorded by the Lake Zigetang pollen spectra. Quaternary International 154–155, 113–121.

Herzschuh, U., Kramer, A., Mischke, S., Zhang, C., 2009. Quantitative climate and vegetation trends since the Late Glacial on the northeastern Tibetan Plateau inferred from Koucha Lake pollen record. Quaternary Research 71, 162–171.

Herzschuh, U., Birks, H.J.B., Mischke, S., Zhang, C., Böhner, J., 2010. A modern pollen-climate calibration set based on lake sediments from the Tibetan Plateau and its application to a

Late Quaternary pollen record from the Qilian Mountains. Journal of Biogeography 37, 752–766.

Herzschuh, U., Borkowski, J., Schewe, J., Mischke, S., Tian, F., 2014. Moisture-advection feedback supports strong early-to-mid Holocene monsoon climate on the eastern Tibetan Plateau as inferred from a pollen-based reconstruction. Paleogeography, Paleoclimatology, Paleoecology 402, 44-54.

Hou, J., D'Andrea, W.J., Liu, Z., 2012. The influence of ^{14}C reservoir age on interpretation of paleolimnological records from the Tibetan Plateau. Quaternary Science Reviews 48, 67-79.

Huang, L., Liu, J., Shao, Q., Liu, R., 2011. Changing inland lakes responding to climate warming in northeastern Tibetan Plateau. Climatic Change 109, 479-502.

IPCC, 2007: Climate Change 2007: The Physical Science Basis. Contribution of Working Group I to the Fourth Assessment Report of the Intergovernmental Panel on Climate Change [Solomon, S., D. Qin, M. Manning, Z. Chen, M. Marquis, K.B. Averyt, M.Tignor and H.L. Miller (eds.)]. Cambridge University Press, Cambridge, United Kingdom and New York, NY, USA.

Jian, X., Guan, P., Zhang, W., Feng, F., 2013. Geochemistry of Mesozoic and Cenozoic sediments in the northern Qaidam basin, northeastern Tibetan Plateau: Implications for provenance and weathering. Chemical Geology, 360-361, 74-88.

Ji, J.f., Shen, J., William, B., Liu, L.W., Liu, X., 2005. Asian monsoon oscillations in the north-eastern Qinghai–Tibet Plateau since the late glacial as interpreted from visible reflec- tance of Qinghai Lake sediments. Earth and Planetary Science Letters 233, 61–70.

Kasper, T., Haberzettl, T., Wang, J., Daut, G., Doberschütz, S., Zhu, L., Mäusbacher, R., 2015. Hydrological variations on the Central Tibetan Plateau since the LGM and thier teleconnections to inter-regional and hemispheric climate variations. Journal of Quaternary Sciences 30. 70-78.

Kaiser, K., 2004. Pedogeomorphological transect studies in Tibet: implications for land-scape history and present-day dynamics. Pr. Geograficzne 200, 147–165.

Kaiser, K., Schoch, W.H., Miehe, G., 2007. Holocene paleosols and colluvial sediments in Northeast Tibet (Qinghai Province, China): properties, dating and paleoenvironmental implications. Catena 69, 91–102.

Kong, P., Na, C.G., Brown, R., Fabel, D., Freeman, S., Xiao, W., Wang, Y.J., 2011. Cosmogenic ^{10}Be and ^{26}Al dating of paleolake shorelines in Tibet. Journal of Asian Earth Sciences 41, 263–273.

Kramer, A., Herzschuh, U., Mischke, S., Zhang, C., 2010a. Late Glacial vegetation and climate oscillations on the south-eastern Tibetan Plateau inferred from the Lake Naleng pollen profile. Quaternary Research 73, 324-335.

Kramer, A., Herzschuh, U., Mischke, S., Zhang C., 2010b. Late Quaternary environmental history of the south-eastern Tibetan Plateau inferred from the Lake Naleng non-pollen palynomorph record. Vegetation History and Archaeobotany 19, 453-468.

Kramer, A., Herzschuh, U., Mischke, S., Zhang C., 2010c. Holocene tree-line shifts and monsoon variability in the Hengduan Mountains (south-eastern Tibetan Plateau) implications from palynological investigations. Palaeogeography, Palaeoclimatology, Palaeoecology 286, 23-41.

Krauskopf, K.B., Bird, D.K., 1995. Introduction to Geochemistry, third ed. WCB/McGraw-Hill, New York, 647pp.

Li Y., Qiang M., Wang G., Li F., Liu Y., Jin Y., Li H., Jin M., 2015. Processes of exogenous detrital input to Genggahai Lake and climatic changes in the Gonghe Basin since the Late Glacial. Quaternary Sciences 35, 160-171,

Liu, C., Masuda, A., Okada, A., Yabuki, S., Zhang, J., Fan, Z., 1993. A geochemical study of loess and desert sand in northern China: implications for continental crust weathering and composition. Chemical Geology 106, 359-374.

Liu, X.J., Lai, Z.P., Zeng, F.M., Madsen, D.B., Yi, C.E., 2013. Holocene lake level variations on the Qinghai-Tibetan Plateau. International Journal of Earth Sciences 102, 2007-2016.

Liu, Y.H., Henderson, G.M., Hu, C.Y., Mason, A.J., Charnley, N., Johnson, K.R., Xie, S.C., 2013b. Links between the East Asian Monsoon and North Atlantic climate during the 8,200 year event. Nature Geosciences 6, 117-120.

Lucchini, F., Dinelli, E., Calanchi, N., 2003. Chemostratigraphy of Lago Albano sediments (Central Italy): geochemical evidence of palaeoenvironmental changes in late Quaternary. Journal of Paleolimnology 29, 109–122.

Meyers, P.A., 1994. Preservation of elemental and isotopic source identification of sedimentary organic matter. Chemical Geology 114, 289–302.

Meyers, P.A., Teranes, J.L., 2001, Sediment organic matter. In: Last, W.M., Smol, J.P. (Eds.), Tracking Environmental Change Using Lake Sediments, vol. 2: Physical and Geochemical Techniques. Kluwer Academic Publishers, Dordrecht, 239–270.

Mischke, S., Kramer, M., Zhang, C., Shang, H., Herzschuh, U., Erzinger, J., 2008. Reduced early Holocene moisture availability in the Bayan Har Mountains, northeastern Tibetan Plateau, inferred from a multiproxy lake record. Palaeogeography, Palaeoclimatology, Palaeoecology 267, 59–76.

Mischke, S., Zhang, C., 2010. Holocene cold events on the Tibetan Plateau. Global and Planetary Change 72, 155-163.

Mischke, S., Aichner, B., Diekmann, B., Herzschuh, U., Plessen, B., Wünnemann, B., Zhang, C., 2010. Ostracods and stable isotopes of a late glacial and Holocene lake record from the NE Tibetan Plateau. Chemical Geology 276, 95–103.

Mischke, S., Weynell, M., Zhang, C., Wiechert, U., 2013. Spatial variability of ^{14}C reservoir effects in Tibetan Plateau lakes. Quaternary International 313-314, 147-155.

Morrill, C., Overpeck, J.T., Cole, J.E., 2003. A synthesis of abrupt changes in the Asian summer monsoon since the last deglaciation. Holocene 13, 465-476.

Nesbitt, H.W., Young, G.M., 1982. Early Proterozoic climates and plate motions inferred from major element chemistry of lutites. Nature 299, 715–717.

Opitz, S., Wünnemann, B., Aichner, B., Dietze, E., Hartmann, K., Herzschuh, U., IJmker, J., Lehmkuhl, F., Li, S., Mischke, S., Plotzki, A., Stauch, G., Diekmann, B., 2012. Late Glacial and Holocene development of Lake Donggi Cona, north-eastern Tibetan Plateau, inferred from sedimentological analysis. Paleogeography, Paleoclimatology, Paleoecology 337-338, 159–176.

Opitz, S., Ramisch, A., Mischke, S., Diekmann, B., 2013. Holocene lake stages and thermokarst dynamics in a discontinuous permafrost affected region, north-eastern Tibetan Plateau. Permafrost and Periglacial Processes, Journal of Asian Earth Sciences 76, 85-94.

Ouimet, W., Whipple, K., Royden, L., Reiners, P., Hodges, K., Pringle, M., 2010. Regional incision of the eastern margin of the Tibetan Plateau. Lithosphere 2, 50–63.

Overpeck, J., Anderson, D., Trumbore, S., Prell, W., 1996. The southwest Indian Monsoon over the last 18 000 years. Climate Dynamics 12, 213-225.

Prell, W.L., Kutzbach, J.E., 1992. Sensitivity of the Indian Monsoon to forcing parameters and implications for its evolution. Nature 360, 647–652.

Reid, A., Fowler, A., Phillips, D., and Wilson, C., 2005, Thermochronology of the Yidun Arc, central eastern Tibetan Plateau: Constraints from Ar/Ar K-feldspar and apatite fission track data: Journal of Asian Earth Sciences 25, 915–935.

Reimer, P.J., Baillie, M.G.L., Bard, E., Bayliss, A., Beck, J.W., Bertrand, C.J.H., Blackwell, P.G., Buck, C.E., Burr, G.S., Cutler, K.B., Damon, P.E., Edwards, R.L., Fairbanks, R.G., Friedrich, M., Guilderson, T.P., Hogg, A.G., Hughen, K.A., Kromer, B., McCormac, F.G., Manning, S.W., Ramsey, C.B., Reimer, R.W., Remmele, S., Southon, J.R., Stuiver, M., Talamo, S., Taylor, F.W., van der Plicht, J., Weyhenmeyer, C.E., 2004. IntCal04 terrestrial radiocarbon age calibration, 26–0 kyr BP. Radiocarbon 46, 1029–1058.

Rosenbaum, J.G., Reynolds, R.L., 2004. Record of Late Pleistocene glaciation and deglaciation in the southern cascade range. II. Flux of glacial flour in a sediment core from Upper Klamath Lake, Oregon. Journal of Paleolimnology 31, 235–252.

Shao, X.H., Wang, Y.J., Cheng, H., Kong, X.G., Wu, J.Y., Lawrence, E.R., 2006. Long-term trend and abrupt events of the Holocene Asian monsoon inferred from a stalagmite δ^{18}O record from Shennongjia in Central China. Chinese Science Bulletin 51, 221–228.

Shao, J., Yang, S., 2012. Does chemical index of alteration (CIA) reflect silicate weathering and monsoonal climate in the Changjiang River basin? Chinese Science Bulletin, 57, 1178-1187.

Shen, J., Liu, X., Wang, S., Ryo, M., 2005. Paleoclimatic changes in the Qinghai Lake area during the last 18,000 years. Quaternary International 136, 131–140.

Shen, C.M., Liu, K.B., Tang, L.Y., Overpeck, J.T., 2006. Quantitative relationships between modern pollen rain and climate in the Tibetan Plateau. Review of Palaeobotany and Palynology 140, 61–77.

Staubwasser, M., Sirocko, F., Grootes, P.M., Segl, M., 2003. Climate change at the 4.2 ka BP termination of the Indus valley civilization and Holocene south Asian monsoon variability. Geophysical Research Letters 30, art. no. 1425.

Strasky, S., Graf. A., Schlüchter, C., Zhao, Z., Ochs, S.I., Kubik, W., Baur, H., Wieler, B., 2007. Evidence for a Late Glacial event in the Kanding area, eastern Tibet. Quaternary International 167–168, 367–368.

Strasky, S., Graf, A., Zhao, Z., Kubik, P.W., Baur, H., Schlüchter, C., Wieler, R., 2009. Late Glacial ice advances in southeast Tibet. Journal of Asia Earth Sciences 34, 458-465.

Stuiver, M., Reimer, P.J., 1993. Extended ^{14}C database and revised CALIB radiocarbon calibration program. Radiocarbon 35, 215–230.

Thompson, L.G., 2000. Ice core evidence for climate change in the Tropics: implications for our future. Quaternary Science Reviews 19, 19–35.

Van Campo, E., Gasse, F., 1993. Pollen- and diatom-inferred climatic and hydrological changes in Sumxi Co Basin (Western Tibet) since 13,000 yr BP. Quaternary Research 39, 300–313.

Wang, Y., Cheng, H., Edwards, R.L., Kong, X., Shao, X., Chen, S., Wu, J., Jiang, X., Wang, X., An, Z., 2008. Millennial- and orbital-scale changes in the East Asian monsoon over the past 224000 years. Nature 451, 1090-1093.

Wang, Y., Herzschuh, U., Shumilovskikh, L., S., Mischke, S., Birks, H., J., B., Wischnewski, J., Böhner, J., Schlütz, F., Lehmkuhl, F., Diekmann, B., Wünnemann, B., Zhang, C., 2013. Quantitative reconstruction of precipitation changes on the NE Tibetan Plateau since the Last Glacial Maximum – extending the concept of pollen source area to pollen based climate reconstructions from large lakes. Climate of the Past Discussion 9, 3563–3613.

Wischnewski, J., Mischke, S., Wang, Y.B., Herzschuh, U., 2011. Reconstructing climate variability on the northeastern Tibetan Plateau since the last Late Glacial – a multi-proxy, dual-site approach comparing terrestrial and aquatic signals, Quaternary Science Reviews 30, 82–97.

Wu, W., Liu, T., 2004. Possible role of the “Holocene Event 3” on the collapse of Neolithic cultures around the central plain of China. Quaternary International 117, 153–166.

Wu, Y., Lücke, A., Jin, Z., Wang, S., Schleser, G.H., Battarbee, R.W., Xia, W., 2006. Holocene climate development on the central Tibetan Plateau: a sedimentary record from Cuoe Lake. Palaeogeography, Palaeoclimatology, Palaeoecology 234, 328–340.

Yu, S.-Y., Zhu, C., Song, J., Qu, W.Z., 2000. Role of climate in the rise and fall of Neolithic cultures on the Yangtze Delta. Boreas 29, 157–165.

Yu, S.Y., Shen, J., Colman, S.M., 2007. Modeling the radiocarbon reservoir effect in lacustrine systems. Radiocarbon 49, 1241-1254.

Yu, S.Y., Ricketts, R., Colman S., 2009. Determining the spatial and temporal patterns of climate changes in China's western interior during the last 15 ka from lacustrine oxygen isotope records. Journal of Quaternary Science, 24, 237–247.

Yu, X., Zhou, W., Franzen, L.G., Xian, F., Cheng, P., Jull, A.J.T., 2006. High-resolution peat records for Holocene monsoon history in the eastern Tibetan Plateau. Science in China Series D 49, 615–621.

Zeng, C., Zhang, F., Wang, Q., Chen, Y., Joswiak, D. R., 2013. Impact of alpine meadow degradation on soil hydraulic properties over the Qinghai-Tibetan Plateau. Journal of Hydrology, 478, 148-156.

Zhang, C., Mischke, S., 2009. A Late Glacial and Holocene lake record from the Nianbaoyeze Mountains and inferences of lake, glacier and climate evolution on the eastern Tibetan Plateau. Quaternary Science Reviews 28, 1970-1983.

Figure Captions:

Fig. 1 Satellite image of Lake Naleng (31.10°N, 99.75°E) located on the south-eastern Tibetan Plateau about 4200 m asl (Landsat 8 scene from May 2013, Band 8 panchromatic, source: http://earthexplorer.usgs.gov). Numbers one to nine indicate sampling points for ^{10}Be surface exposure dating from erratic boulders from inner, middle, lateral, and outer end moraines. The calculated erosion corrected ages for the separate sampling points are : 1. 21.6 ± 1.0 ka BP; 2. 21.2 ± 1.0 ka BP; 3. 20.7 ± 0.9 ka BP; 4. 20.1 ± 1.0 ka BP; 5. 17.6 ± 0.7 ka BP; 6. 18.9 ± 0.8 ka BP; 7. 19.5 ± 1.0 ka BP; 8. 17.5 ± 0.7 ka BP; 9. 22.0 ± 0.9 ka BP (Strasky et al., 2009).

Fig. 2 Lithological overview of the investigated sediment core from Lake Naleng based on

Kramer et al. (2010b, c) at left, and total organic carbon (TOC), C/N ratio, $\delta^{13}C_{org}$ and reconstructed mean annual precipitation (MAP) and mean annual temperature (MAT) based on pollen assemblages of Kramer et al. (2010b; dashed line indicates mean value)

Fig. 3 Mean grain size and clay (<2 μm), silt (2–63 μm) and sand (>63 μm) fractions for the sediment core from Lake Naleng.

Fig. 4 Weathering parameters (Y/Al; CIA; Sr/Ba; Al/Rb) and low frequency magnetic susceptibility (χ_{LF}) of the Lake Naleng record.

Fig. 5 Concentrations of major elements in weight percentage (wt%) and Mg/Ca ratios revealed by XRF analysis for the last 17.7 cal ka BP at Lake Naleng.

Fig. 6 Principal component analyses (PCA) biplot of the complete dataset from Lake Naleng.

Figure 1
Click here to download high resolution image

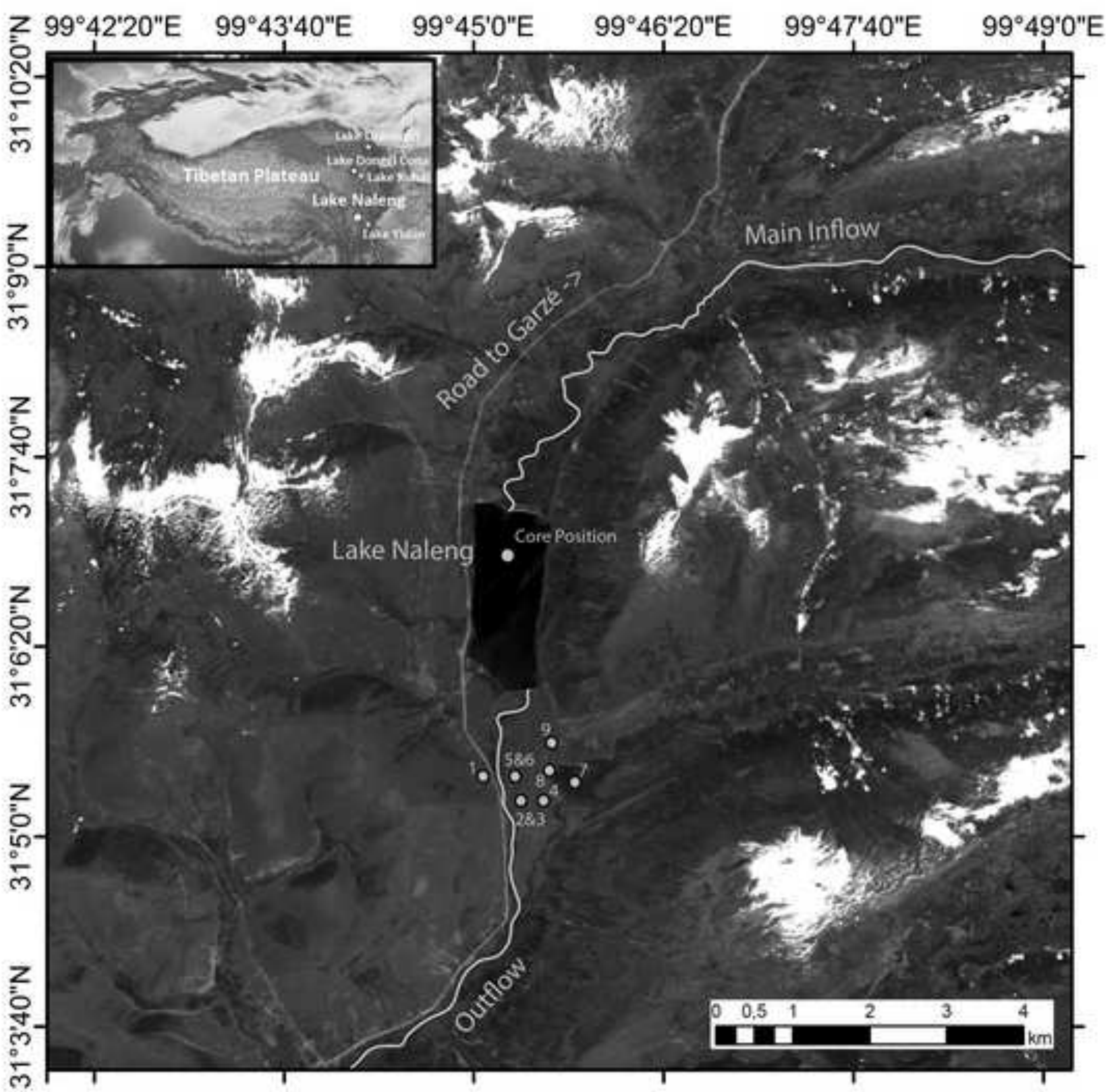

Figure 2

Click here to download high resolution image

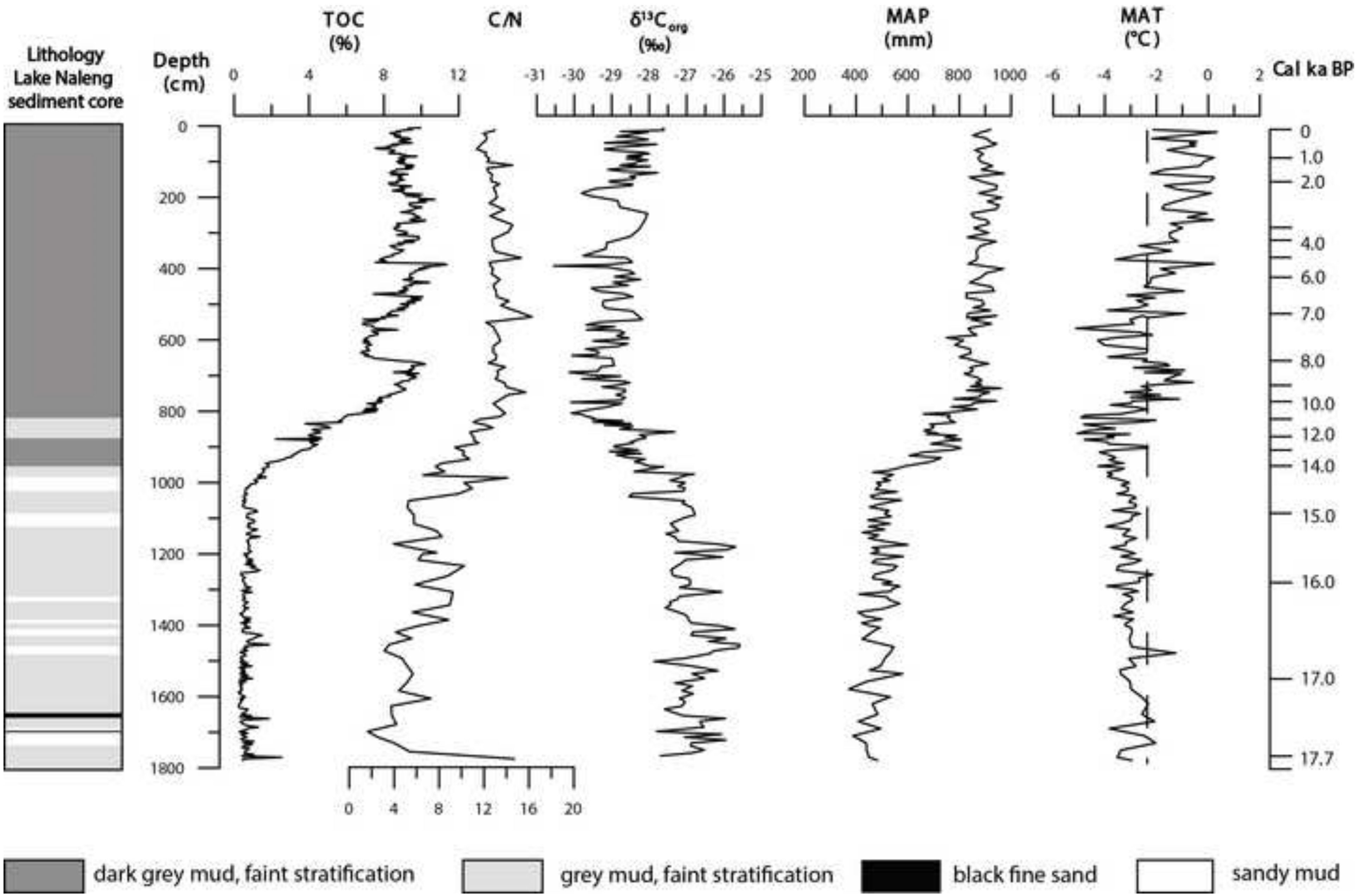

Figure 3
Click here to download high resolution image

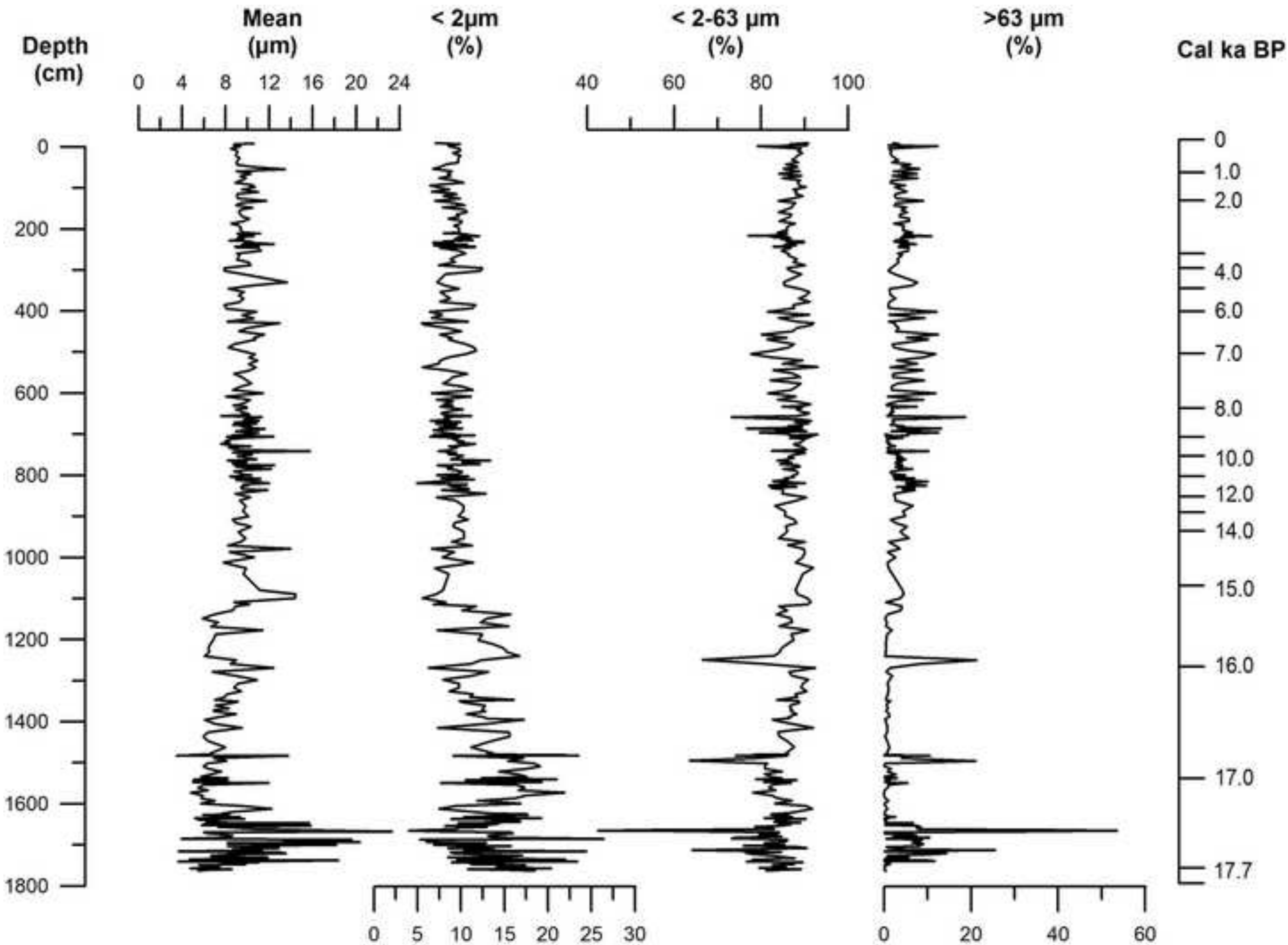

Figure 4
Click here to download high resolution image

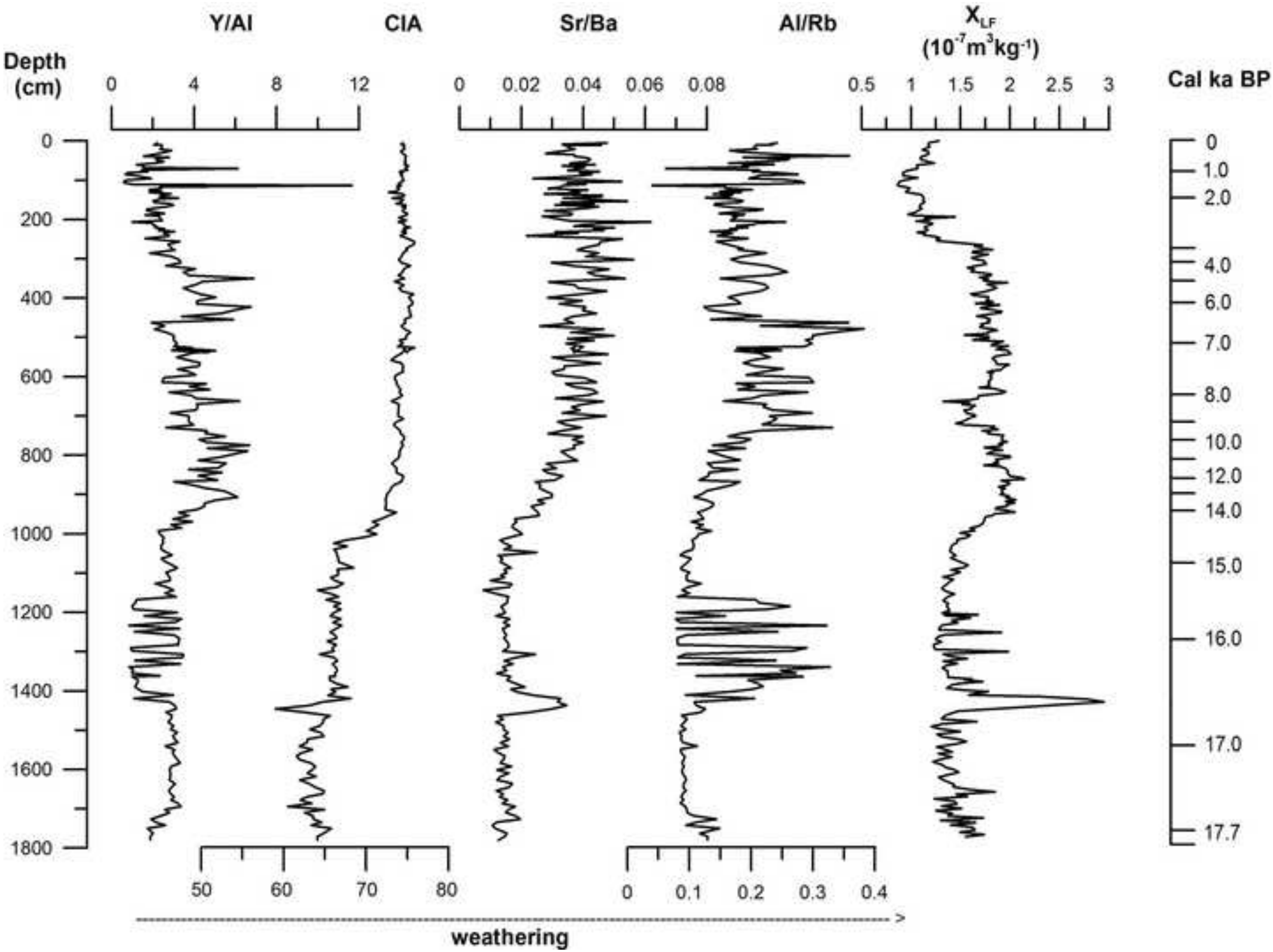

Figure 5

Click here to download high resolution image

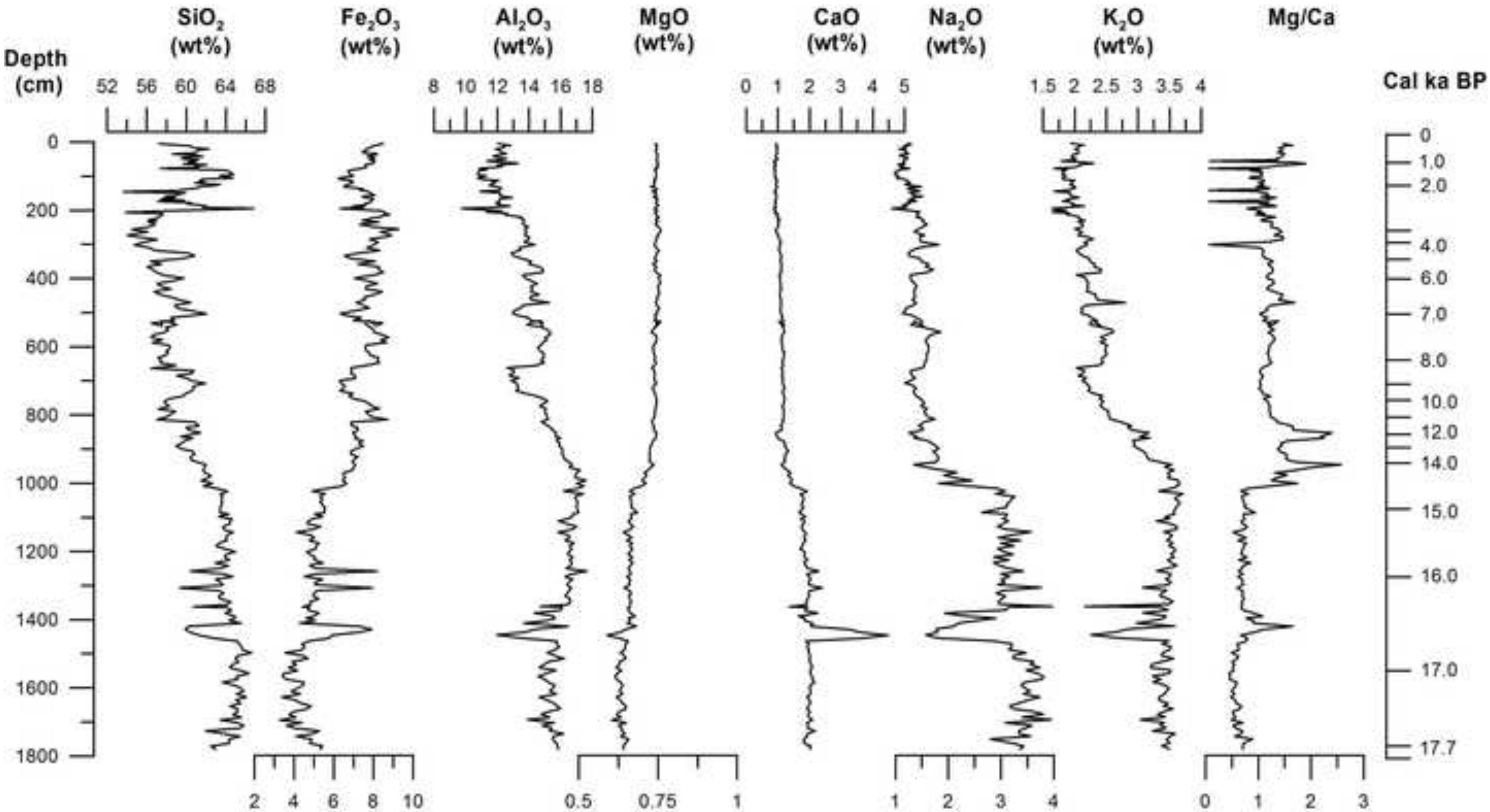

Figure 6

Click here to download high resolution image

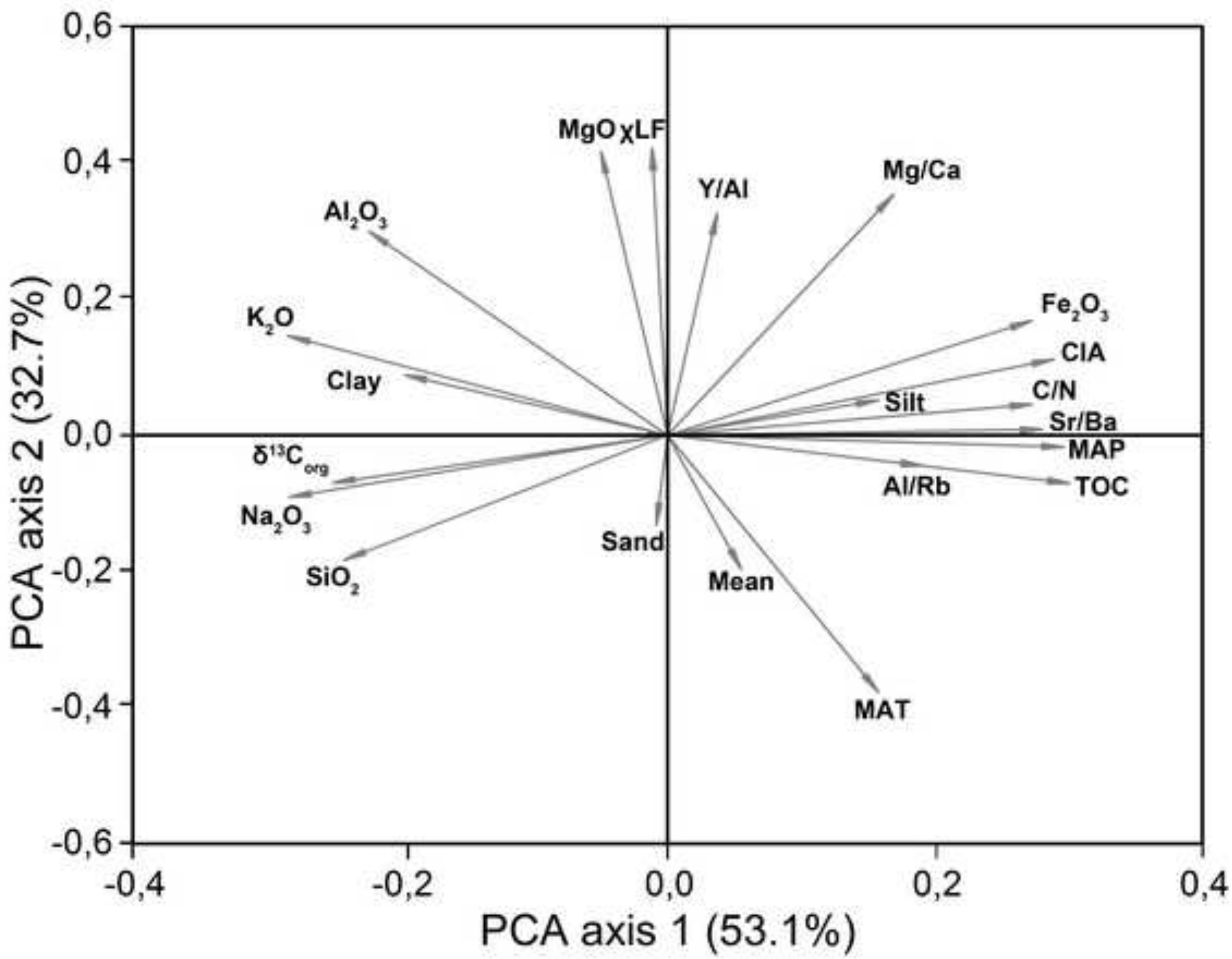

KML File (for GoogleMaps)

Click here to download KML File (for GoogleMaps): Lake Naleng.kmz